Evolution of a calcite marble shear zone complex on Thassos Island, Greece: microstructural and textural fabrics and their kinematic significance

Michel Bestmann[a,*], Karsten Kunze[b], Alan Matthews[c]

[a]*Institut für Geologie und Mineralogie, Schloßgarten 5, D-91054 Erlangen, Germany*
[b]*Geologisches Institut, ETH Zentrum, Sonneggstr. 5, CH-8092 Zürich, Switzerland*
[c]*Institute of Earth Sciences, Hebrew University of Jerusalem, 91904 Jerusalem, Israel*

Abstract

The deformation history of a monophase calcite marble shear zone complex on Thassos Island, Northern Greece, is reconstructed by detailed geometric studies of the textural and microstructural patterns relative to a fixed reference system (shear zone boundary, SZB). Strain localization within the massive marble complex is linked to decreasing $P–T$ conditions during the exhumation process of the metamorphic core complex. Solvus thermometry indicates that temperatures of 300–350°C prevailed during part of the shear zone deformation history. The coarse-grained marble protolith outside the shear zone is characterized by symmetrically oriented twin sets due to early coaxial deformation. A component of heterogeneous non-coaxial deformation is first recorded within the adjacent protomylonite. Enhanced strain weakening by dynamic recrystallization promoted strong localization of plastic deformation in the ultramylonite of the calcite shear zone, where high strain was accommodated by non-coaxial flow. This study demonstrates that both a pure shear and a simple shear strain path can result in similar crystallographic preferred orientations (single c-axis maximum perpendicular to the SZB) by different dominant deformation mechanisms. Separated a-axis pole figures ($+a$- and $-a$-axis) show different density distributions with orthorhombic texture symmetry in the protolith marble and monoclinic symmetry in the ultramylonite marble consistently with the observed grain fabric symmetry. © 2000 Elsevier Science Ltd. All rights reserved.

1. Introduction

Carbonate rocks are able to accumulate large amounts of strain, and deform crystal-plastically even at low $P–T$ conditions. The minimum temperature for crystal plasticity of calcite is about 180°C (Burkhard, 1990), whereas, e.g. quartz shows plastic flow not below 270°C (e.g. Voll, 1976), and feldspar above 450–500°C (Tullis, 1983). Particularly in carbonate rich orogenic belts, e.g. the Alps, marbles can record plastic tectonic processes in the upper crust and thus the localization of plastic flow in carbonate shear zones is an important process in lithosphere dynamics. The understanding of shear zone evolution in carbonates may also be extrapolated to localization phenomena in other rock types, which are less accessible. Microfabric (microstructure and texture) studies in marble shear zones provide data about the physical conditions, kinematics and processes of deformation.

Shear zones are narrow, planar, subparallel-sided domains where strain was locally concentrated relative to their surrounding regions (Ramsay, 1980). Mylonitic rocks within a shear zone complex are commonly characterized by tectonically reduced grain size relative to their protolith caused by dynamic recrystallization. Crystallographic preferred orientation (CPO, texture) usually develops during the crystal–plastic deformation process.

The symmetry of microfabrics with respect to a reference frame is a significant property for deduction of the kinematics in the deformation history of a shear zone complex (e.g. Paterson and Weiss, 1961; Wenk and Christie, 1991; Means, 1994). Such sample reference frame should relate to kinematic features like the shear zone boundary (shear plane) and the shear direction within that plane. However, the shear plane is rarely exposed in the field, and the foliation is usually considered as the reference plane, which is often in an (unknown) oblique angle to the kinematic framework of a shear zone. For an interpretation of the strain path (e.g. pure shear vs. simple shear) both microstructures and textures have to be studied. The symmetry of the
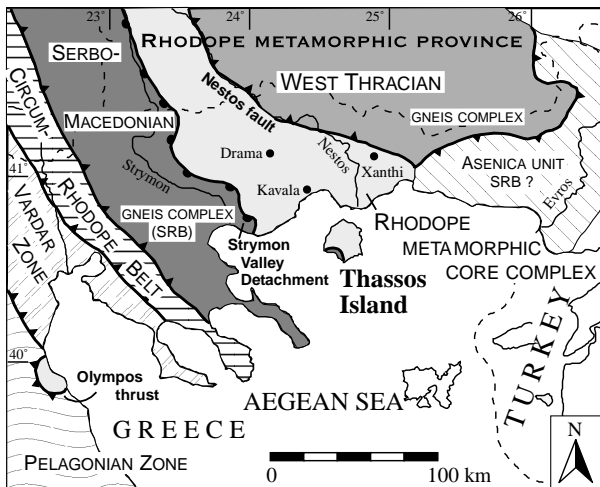
Fig. 1. Tectonometamorphic map of the north Aegean region (NE Greece) showing the structural setting of the south Rhodope area (simplified and compiled after Papanikolaou, 1984; Dinter, 1998; Kilias et al., 1999).

deformation regime (strain path) is reflected in the symmetry of the resultant crystallographic and grain shape fabric. In general, monoclinic textures are interpreted as indicators for simple shear, while pure shear results in orthorhombic symmetry of the fabric (e.g. Wenk et al., 1987).

This study presents a systematic microstructural and textural analysis of a shear zone in a calcite marble complex located in the Thassos Island metamorphic core complex, Northern Greece (Fig. 1). Regional aspects of tectonics, regional geology and geochronology of this core complex are well defined (e.g. Schulz, 1992; Peterek et al., 1994; Wawrzenitz and Krohe, 1998). The shear zone complex provides an ideal framework for detailed analysis of the processes active during the tectonic event: (1) mono-mineralic composition across the shear zone complex, (2) well-developed tectonic elements (both macro- and micro-fabrics), (3) relatively simple geometry, and (4) accessibility to well-exposed section. Monophase rocks are commonly favoured for microfabric investigation, because intermineralic reactions and rheological interaction of different mineral phases can be excluded.

A complete sequence of differently strained calcite marbles is examined, ranging from the relatively 'low-strained' and coarse-grained protolith outside the shear zone to highly strained and fine-grained ultramylonite in the center of the shear zone. The microstructures were analyzed using optical microscopy. Textures were determined by neutron goniometry and by individual orientation measurements using electron backscatter diffraction (EBSD). The data of the shear zone complex were compared to results from published experimental deformation and numerical modeling studies. The temperatures during the shear zone formation were assessed from electron-microprobe analyses and calcite–dolomite solvus thermometry.

2. Geological setting and sample location

The studied shear zone is located on Thassos Island in the northern Aegean Sea of Greece. Most parts of the metamorphic succession of Thassos Island are related to the Rhodope metamorphic core complex (Fig. 1). The Thassos Island crystalline complex is made up of three superimposed tectonic units (lower, intermediate, and upper unit, Fig. 2) with geochronologic ages decreasing downwards (Wawrzenitz and Krohe, 1998). These tectonic units are separated by two SW-dipping low-angle normal fault systems (Dinter and Royden, 1993; Peterek et al., 1994; Wawrzenitz and Krohe, 1998). The metamorphic succession is dominated by massive marble complexes alternating with paragneisses, orthogneisses, and amphibolites (e.g. Peterek et al., 1994). In response to crustal thickening during Alpine tectonics (Dinter, 1998), the maximum metamorphic conditions were estimated of approximately 620°C/4.7kbar for the lower unit and 580°C/2.4kbar for the intermediate unit, as determined by geothermobarometric analyses of amphibole gneisses (unpublished data and recalculated data of Schulz, 1992). Penetrative shearing during crustal uplift produced a main extensional fabric overprinting older compressive structures within the metamorphic succession, under retrograde metamorphic conditions (Peterek et al., 1994). Characteristic of this process is the development of NE–SW-trending mineral lineation with a top-to-SW oriented sense of shear. Rb–Sr analyses of whole-rock data and white mica constrain the onset of extensional deformation at 26 Ma and ongoing deformation at 23–24 Ma (Wawrzenitz and Krohe, 1998). This event is considered by Wawrzenitz and Krohe (1998) to be associated with decoupling of the brittle hanging wall (Migmatitic Thassos succession) from the plastically flowing deeper crust (Thassos Falakron succession) (Fig. 2). After deformation under middle crust conditions, the Thassos Falakron succession was separated into an intermediate and a lower unit during continuous uplift of the metamorphic core complex. The decoupling took place along a SW-dipping low-angle normal detachment zone (Wawrzenitz and Krohe, 1998), cutting through a massive marble complex (Profitis Ilias Marble, Fig. 2).

Strain localization corresponded to decreasing P–T conditions during continuing extensional tectonics and linked to the exhumation process of the metamorphic core complex. In the pure calcite marble complexes of the intermediate unit, this stage of deformation is recorded by several shear zones of up to 3 m thickness that are oriented parallel to the foliation plane in the host rocks. During the fragmentation of the intermediate unit, these features are passively rotated or dragged along high angle normal faults. The strain localization event thus preceded the faulting process. Mylonitic deformation in the intermediate unit is considered to have continued in the transitional field between plastic and brittle behaviour of rocks until 15 Ma ago (Rb–Sr dates of biotite, Wawrzenitz and Krohe, 1998).

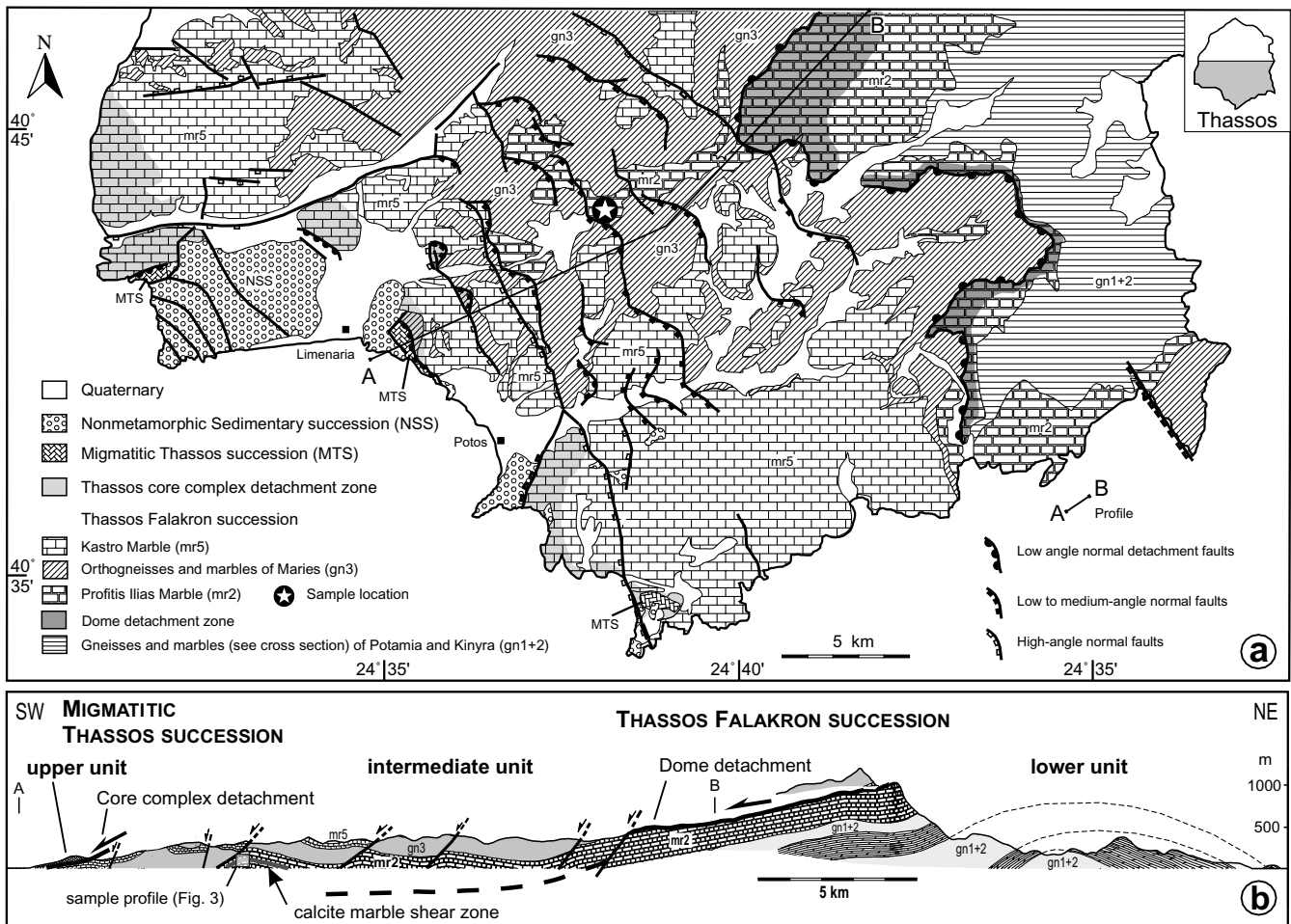Samples were taken from a prominent 2–4 m thick shear

Fig. 2. (a) Geological map of the southern part of Thassos Island, Greece. The sample location indicates the shear zone studied in this work. (b) Geological cross-section through the Thassos Island crystalline complex and geotectonic position of the investigated shear zone. (Compiled after Peterek et al., 1994; Wawrzenitz and Krohe, 1998; Bestmann, 2000.)

zone located within the Profitis Ilias Marble of the intermediate unit, in the SW of Thassos Island, 9 km ENE from Limenaria in the Kastro valley (Fig. 2). The shear zone boundaries are parallel to the main foliation of the coarse-grained calcite marble. The base of the calcite marble complex is not exposed. The contact with the overlying gneiss is 180 m above the marble shear zone. This marble sequence is fragmented by SW-dipping high angle normal faults associated with block-tilting. The small-scale shear zones are present throughout the marble fragments at the same structural level. Rare mica flakes in the coarse-grained marble define a mineral lineation parallel to that present in the country rock gneisses (dip direction 210°). The intensity of mylonitization varies within the shear zone from anastomosing centimeter-scale shear bands up to homogeneous fine-grained ultramylonitic layers of few meters thickness.

For the detailed laboratory studies, sampling was carried out along a creek where the shear zone is well exposed. A schematic profile across the shear zone complex is given in Fig. 3. The upper and lower contacts (= shear zone

boundaries) between the very fine-grained ultramylonite and the coarse-grained protolith are sharp. Protomylonitic fabrics occur in the coarse-grained marble at these contacts. The ultramylonite is uniformly fine-grained, except for a 60-cm thick intercalated layer of coarse-grained protomylonite, which shows sharp contacts with the ultramylonites. A mineral lineation is not observed within the ultramylonite layers. The most prominent features of the very homogeneous grey ultramylonite are the parallel white layers which are aligned parallel to the shear zone boundary plane and to the main foliation of the protolith (225/08, dip direction/dip). Continuous series of oriented samples were collected, from a 4.5 m channel perpendicular to the SZB planes (Fig. 3).

3. Reference system

Crystallographic and shape fabrics describe preferred orientations with respect to a fixed sample reference system. Conventionally the main foliation is used as the reference
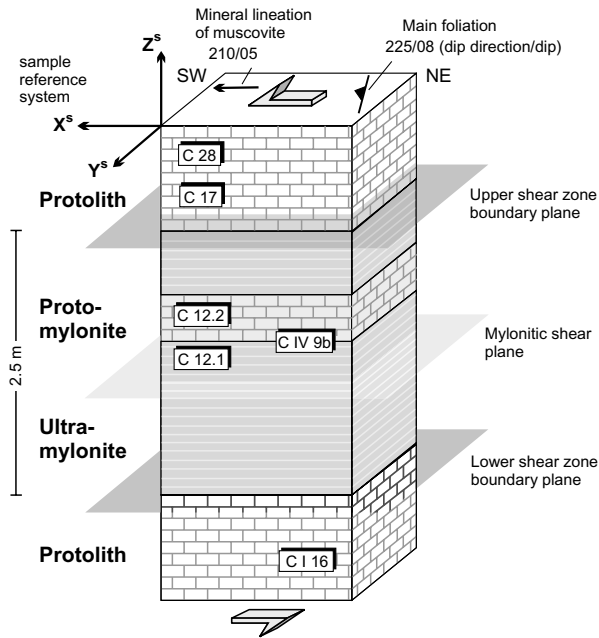
Fig. 3. Sketch of the continuous profile through the shear zone complex. Sample numbers mentioned in the text and figures are indicated. Sample reference system (X^s, Y^s, Z^s) and bulk shear sense (sinistral) are given.

plane. In a shear zone profile, the main foliation is usually oblique to the shear zone boundary and the direction of shear, and rotates towards to those with increasing amount of deformation. The shear zone boundary is a more suitable reference plane, although this is not always exposed in the field. In this study the shear zone boundary plane in combination with the lineation is used as the sample reference system. In case of the Thassos shear zone, both the main foliation of the marble protolith and the mylonitic shear plane are parallel to the shear zone boundary (Fig. 3). Thus, the geometric orientation of this external reference plane contains all the main tectonic planes of the shear zone complex.

In this study, the axes of the sample reference frame are defined by X^s parallel to the mineral lineation, Z^s normal to the shear zone boundary, and Y^s perpendicular to both as marked in Fig. 3. All microstructural observations, photomicrographs and pole figures are presented in X^sZ^s-sections unless otherwise noted. Microstructural fabric orientations are specified with their angular deflection in a clockwise or anticlockwise sense related to the reference plane (X^sY^s-plane). The shear sense was deduced from the geometry of 'σ-shaped' quartz grains incorporated within the calcite matrix of the ultramylonite. Crystallographic orientations

describe the rotation of a crystal fixed coordinate system relative to the sample reference frame. The crystal frame (X^c, Y^c, Z^c) is given with respect to the crystal lattice planes and directions in Fig. 12.

4. Microfabrics

The shear zone developed within a pure calcite marble complex contains generally less than 1 wt.% non-carbonate material. The shear zone complex is subdivided into three marble types recording different strain intensities. The nomenclature is based on the proportion of dynamically recrystallized grains (rexx, for description see Section 4.2.1 and Fig. 7) in the bulk rock (after Sibson, 1977): protolith (<10% rexx), protomylonite (10–50% rexx) and ultramylonite (>90% rexx). Mylonite (50–90% rexx) is absent because of the abrupt transition from protolith and/or protomylonite to the ultramylonite.

The shape of accessory quartz grains within the different marble types indicate uniquely the kinematics of the deformation and are described separately. The first appearance of dolomite in the ultramylonite is used to deduce the temperature range of the shear zone deformation.
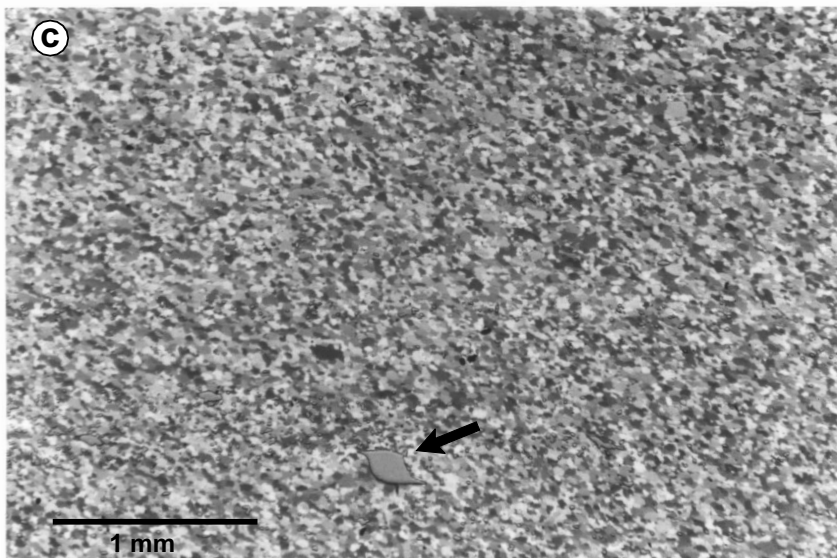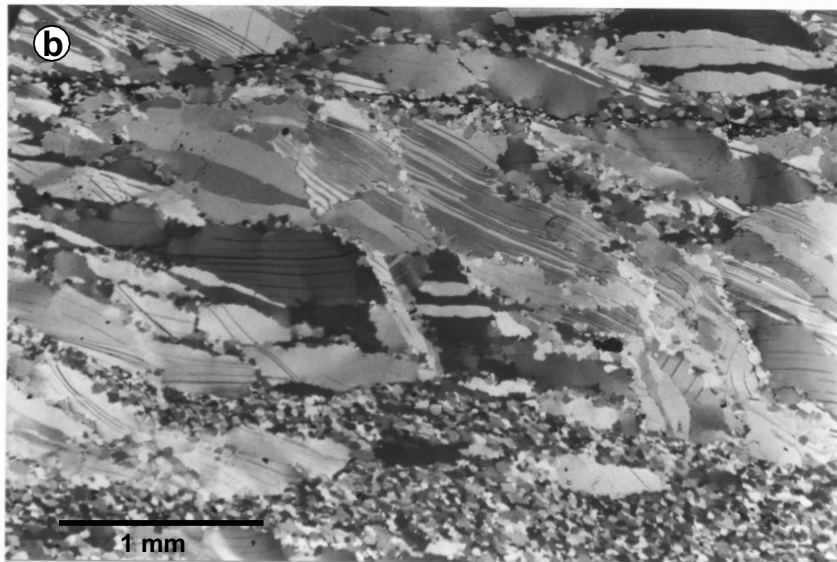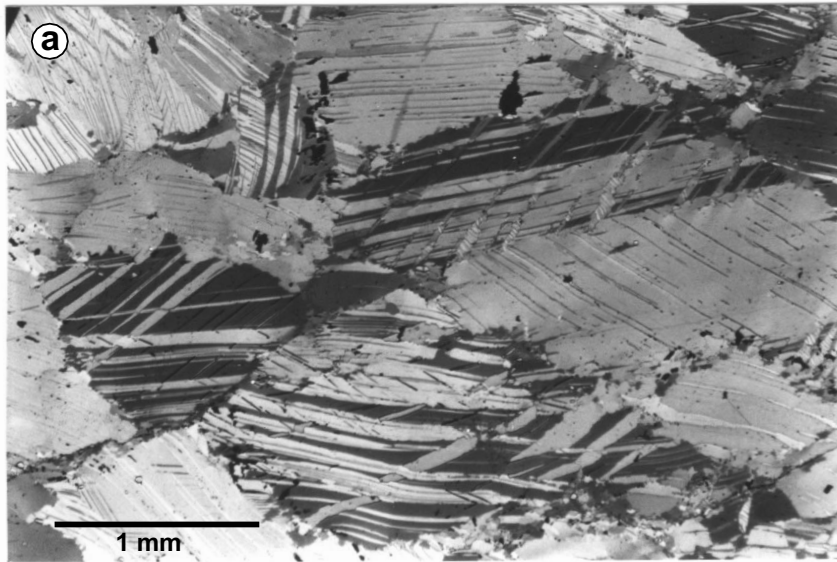
4.1. Protolith

Outside the shear zone the coarse-grained marble protolith shows decimeter to meter wide bedding. Faint colour banding (grey–blue and white) defines a macroscopic main foliation. Variations in cathodoluminescence (CL) intensity occur normal to the layers (see Bestmann, 2000). These CL gradients are not related to specific microstructures observed by transmitted light microscopy. Rare white mica flakes define a mineral lineation striking SW–NE on the bedding and/or foliation plane.

4.1.1. Microstructure

The grain fabric of the marble protolith outside the shear zone is equigranular and coarse-grained with high twin lamellae density (Fig. 4a). The grain size varies between 1–3 mm with a mean axial ratio of 1:1.4. The large grain size of the calcite marble can be related to high temperatures under amphibolite facies metamorphic conditions (Covey-Crump and Rutter, 1989) at an earlier stage. The long axes are oriented approximately in the main foliation plane. The protolith shows a mosaic of rhombic grains with conjugate grain boundaries oriented at an angle of 35° to the long axes. The grain interiors exhibit prominent twinning. Traces of two equally developed sets of twins are oriented clockwise

Fig. 4. Photomicrographs of the three marble types showing different strain intensities. (a) Coarse-grained protolith (C 28) with three sets of twins oriented both clockwise and anticlockwise, and subparallel to the reference plane. (b) Coarse-grained protomylonite (C 12.2) showing a variable intensity of dynamic recrystallization; coarse-grained porphyroclasts are elongated and show a shape preferred orientation, with one dominant twin set clockwise oriented to the reference plane. (c) Penetrative dynamically recrystallized fine-grained ultramylonite (C 12.1); shear sense (sinistral) is given by 'σ-shaped' quartz grains (arrow) embedded within the calcite matrix. Photomicrographs are made in the reflected light mode of the polarization microscope from ultra-high polished slabs in the X^sZ^s-section.
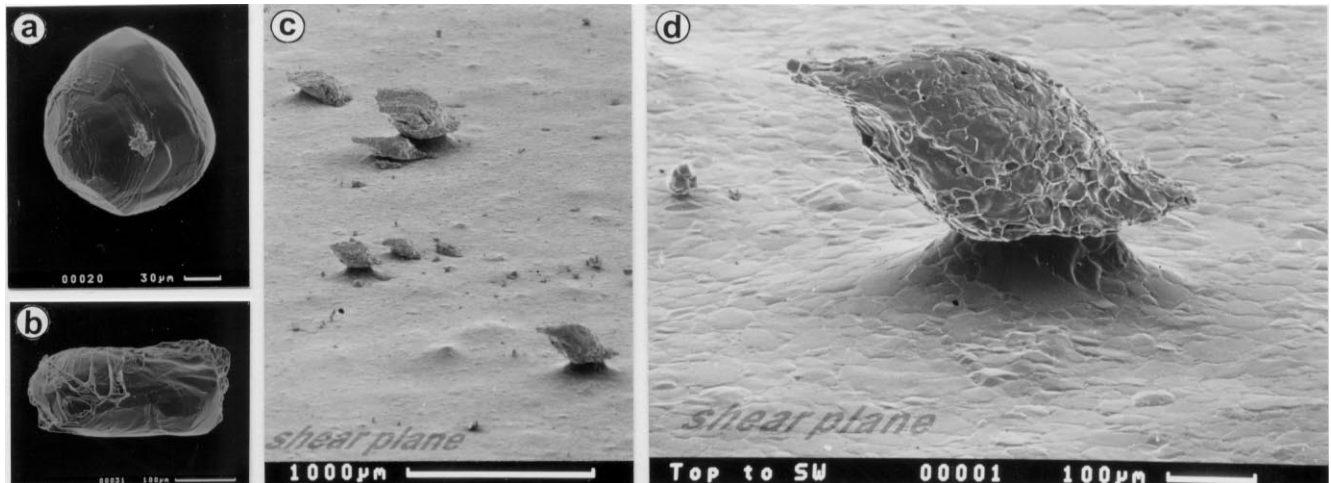
Fig. 5. SEM-photographs of quartz grains incorporated within the calcite marble rocks extracted by etching. (a, b) Quartz grains with different shapes in the protolith and protomylonite marble. (c, d) SEM-photographs of 'σ-shaped' quartz grains situated *in situ* on the surface of the ultramylonitic shear plane. The geometry of the quartz grains indicates a dominant non-coaxial deformation of the ultramylonite marble, with shear direction of the hanging wall towards SW. The surface network reflects the positive relief of the dissolved calcite fabric of the ultramylonitic matrix (grain boundary network).

and anticlockwise with respect to the long axes, and the traces of a third set, less abundant, are subparallel to the grain long axes. Generally the twins terminate at grain boundaries, but some taper to a fine point in the grain interior. Many of the twins are bent smoothly and become narrower towards grain boundary, or have lensoid shapes. Undulose extinction is common. Small calcite grains (10–30 μm) are only evident at few places along the grain boundaries and the twin lamellae of the coarse grains. These small grains show no undulose extinction and no twins.

4.1.2. Quartz grains

Rare quartz grains (50–150 μm) are incorporated in the interior of calcite grains or at grain boundaries. These single grains exhibit undulose extinction. SEM images of individual grains, which are extracted by etching, reveal spherical (Fig. 5a), and ellipsoidal/oblong (Fig. 5b) shapes.

4.1.3. Texture

Two cylindrical samples (C 28, C 17; ~10 cm³ volume) of the coarse marble protolith were studied at the pulsed reactor IBR-2 of the Frank Laboratory of Neutron Physics at Dubna (Russia) by means of time-of-flight (TOF) neutron diffraction, using the high-resolution SKAT texture diffractometer (Ullemeyer et al., 1998). Due to the low absorption of neutrons in matter, large sample volumes of coarser grained rocks can be investigated. Six incomplete pole figures (01-12), (10-14), (0006), (11-20), (11-23) and (01-18) + (02-14) were extracted from the TOF patterns and used as input to calculate the orientation distribution function (ODF) applying the WIMV algorithm as implemented in the BEARTEX program package (Matthies and Vinel, 1982; Wenk et al., 1998). From the ODF, the pole

figures of interest for the kinematic interpretation were recalculated.

Both samples show similar pole figures (Fig. 6a). The *c*-axis (0001) pole figures reveal a single point maximum parallel (C 28) or slightly oblique (C 17) to the normal (Z^s-axis) of the reference shear zone plane. The c-axes define a partial girdle sub-normal to the lineation (X^s-axis). Both the *c*-axis pole figures show a slight asymmetry of the girdle distribution with respect to the Y^sZ^s-plane of the reference system, but of different orientation. For both samples the different *a*-axes ($+a$ [-1-120] and $-a$ [11-20]) show a girdle distribution within the SZB plane normal to Z^s. A maximum is aligned nearly parallel to the shear direction. The separated a-axis pole figures ($+a$ and $-a$) are very similar to each other in both samples. The texture symmetry of the protolith can be generally described as orthorhombic with only slight deviations.

4.2. Protomylonite

4.2.1. Microstructure

Intense grain size reduction characterizes the transition from the protolith to the protomylonite. The grain fabric of the protomylonite is mainly characterized by large calcite porphyroclasts surrounded by equant small grains known as a 'core and mantle' structure (Fig. 4b).

Grain size reduction is evident along grain boundaries and creates conjugate bands with small grains, referred to as recrystallization bands (Fig. 7). With respect to the sinistral sense of the bulk shear, the bands, which are inclined in a clockwise sense by ca. 30°, to the reference plane, are the dominant set. Fig. 7 shows an orientation mapping (Adams et al., 1993) across such a recrystallization band using the EBSD technique in the scanning electron microscope (see Section 4.3.3). Grain and subgrain boundaries are detected
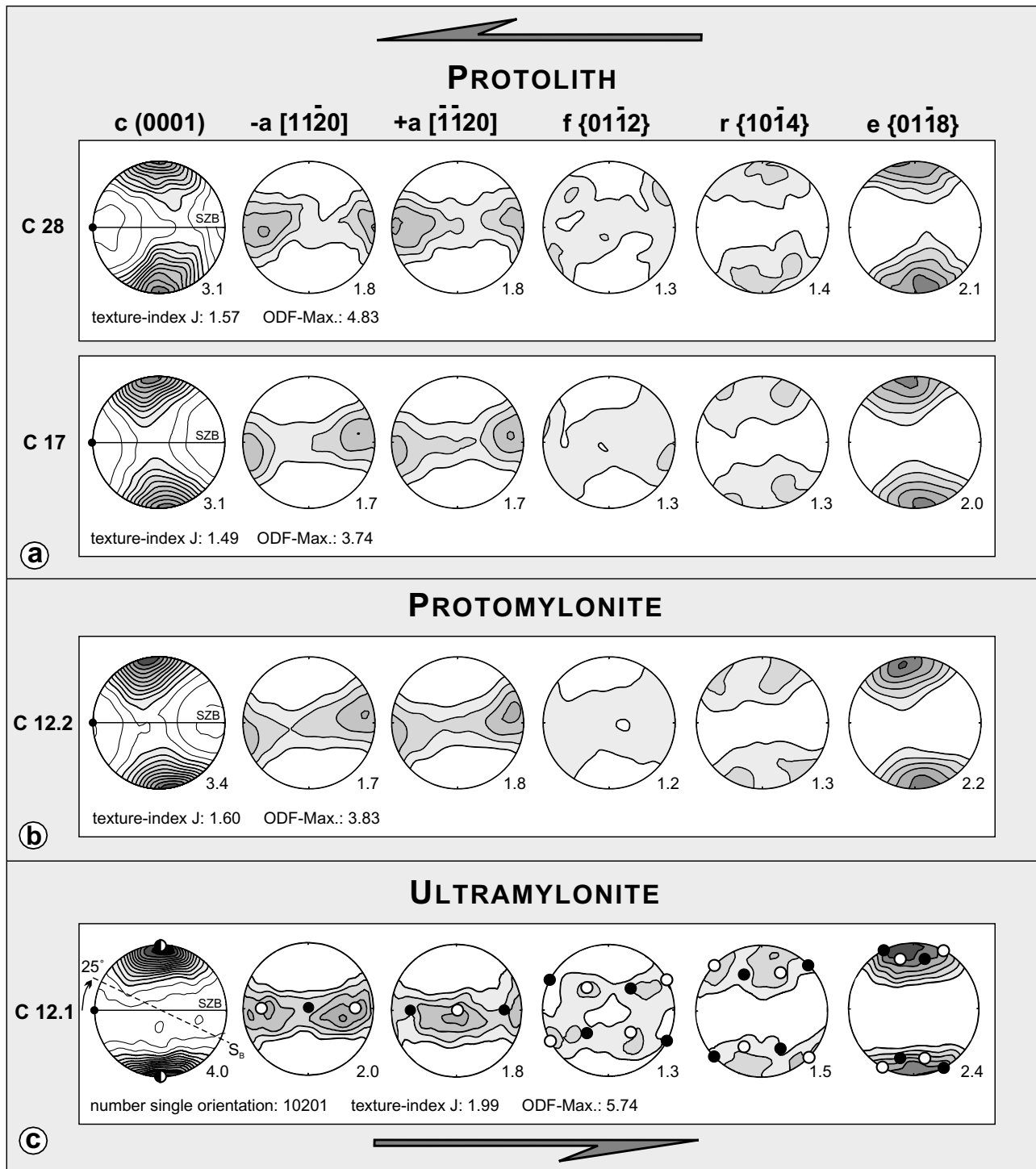
Fig. 6. CPO across the shear zone. (a) Protolith (C 28, C 17), (b) protomylonite (C 12.2), (c) ultramylonite (C 12.1). Equal area, upper hemisphere projection normal to shear zone boundary (SZB) plane, shear direction marked by dot, sinistral sense of shear. S_B: oblique foliation defined by the SPO of dynamically recrystallized grains. Ideal orientations g_A and g_B (Fig. 12a) highlighted by white and black circles, respectively. Lowest shaded contour equal to 1.0 times random, contour intervals 0.25 times random. ODF and pole figure calculations (15° smoothing) using BEARTEX (Wenk et al., 1998). Texture strength characterized by maximum of ODF f(g) and texture index $J = \int f^2(g) dg$.

by analysing the crystallographic mismatch of nearest neighbour orientations (misorientation angle ω_{mn}: rotation angle between two orientations g_m, g_n; e.g. Kunze et al., 1994). Two observations should be highlighted. (1) The upper right clast shows a relatively low amount of lattice misorientation in the interior, but a high number of lowest angle ($1° < \omega_{mn} < 5°$) and low angle ($5° < \omega_{mn} < 15°$) boundaries near the recrystallization band. (2) Within the
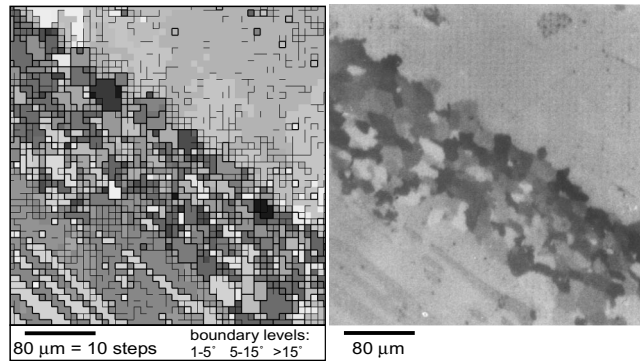
Fig. 7. Orientation mapping by means of automated EBSD (see Section 4.3.3) across a recrystallization band. Boundary levels are detected by analysing the crystallographic mismatch of nearest neighbour pairs (see text) and presented as different thick line segments.

recrystallization band, small grains are separated by high-angle boundaries ($\omega_{mn} > 15°$) and contain few low-angle and lowest-angle boundaries. These grains are generally not twinned and the extinction is sharp, and are referred to as dynamically recrystallized grains with a low internal defect density (see also Section 6.1.2). The grain sizes range between 10 and 50 μm, and elongation parallel to the orientation of the respective recrystallization band is common (Fig. 7). Some recrystallization bands are oriented parallel or slightly oblique to the reference plane. These 100–500 μm thick bands are characterized by a smaller grain size between 5 and 20 μm. Long axes of these small grains are oriented clockwise to the reference plane making an angle of 10–30° and define an oblique foliation (see also Section 4.3.1). No shape preferred orientation is evident in sections perpendicular to the shear direction (Y^sZ^s-section). Some patches of small grains slightly away from the high strain shear zone have larger grain sizes of 50–100 μm. These grains are polygonal without any preferred shape orientation (SPO). All the small grains have straight to slightly curved grain boundaries.

With respect to the protolith the aspect ratio of the coarse calcite porphyroclasts in the protomylonite increased to a mean value of 1:2. The long axes are between 1 and 4.5 mm in length and are typically clockwise oriented with respect to the reference plane at an angle of 25–45° (Fig. 4b). With increasing amount of small grains, flattening of the porphyroclasts is evident and the mean axial ratio increases up to 1:4, with long axis oriented subparallel to the reference plane. Traces of conjugate sets of twins are oriented at low angles (15–35°) anticlockwise and clockwise relative to the reference plane. Clockwise oriented twins dominate and represent the characteristic deformation structure of the porphyroclasts. Many of the twins are lensoid bent or taper in the grain interior. Clockwise oriented twins near the edge of the grains are frequently bent towards the direction of the foliation and display a sigmoidal pattern. Some of the porphyroclasts seem to be almost completely twinned. Twins oriented at a high angle to the reference plane contain secondary twins of the dominant twin set. The thick twins have bulges and irregular twin boundaries, whereas thin

twins are straight. Many porphyroclasts show a characteristic symmetrical undulose extinction by movement of conjugate extinction bands through the grain interior. A flattening parallel to the reference plane characterizes the porphyroclast fabric in the Y^sZ^s-section. Quartz grains within the protomylonite show the same equant shapes as in the protolith.

The oblique microstructural features of the protomylonite marble possess a monoclinic symmetry with respect to the sample reference system.

4.2.2. Texture

The texture of the mainly coarse-grained protomylonite sample (C 12.2, Fig. 6b) as determined by neutron diffraction, is similar to that of the protolith samples, especially to sample C 17. The c-axis maximum and corresponding a-axis girdle reveal an orthorhombic texture symmetry with slightly rotated symmetry axes about the Y^s-axis. Strictly speaking, the texture has only monoclinic symmetry with respect to the reference frame.

4.3. Ultramylonite

The transition from the coarse-grained protolith or proto-mylonite to the fine-grained ultramylonite is in general abrupt, with a sharp contact that defines the shear zone boundary. The homogeneous fine-grained grey ultramylonite marks the interior of the shear zone. The mesoscopical shear plane is defined by a lamination of colour variation, which is visible parallel to the layer in polished specimen slabs. Small white 'streaks' within the grey matrix are aligned parallel to the reference plane. Generally, the streaks are 0.1–3 mm thick and smear out after a few centimeters; rarely do they continue for several decimeters. Cathodoluminescence microscopy indicates a lamination pattern of different luminescence intensity corresponding to the mesoscopical pattern (see Bestmann, 2000).

4.3.1. Microstructure

The fine-grained ultramylonite shows a homogeneous microstructure. In X^sZ^s-sections most of the grains show a
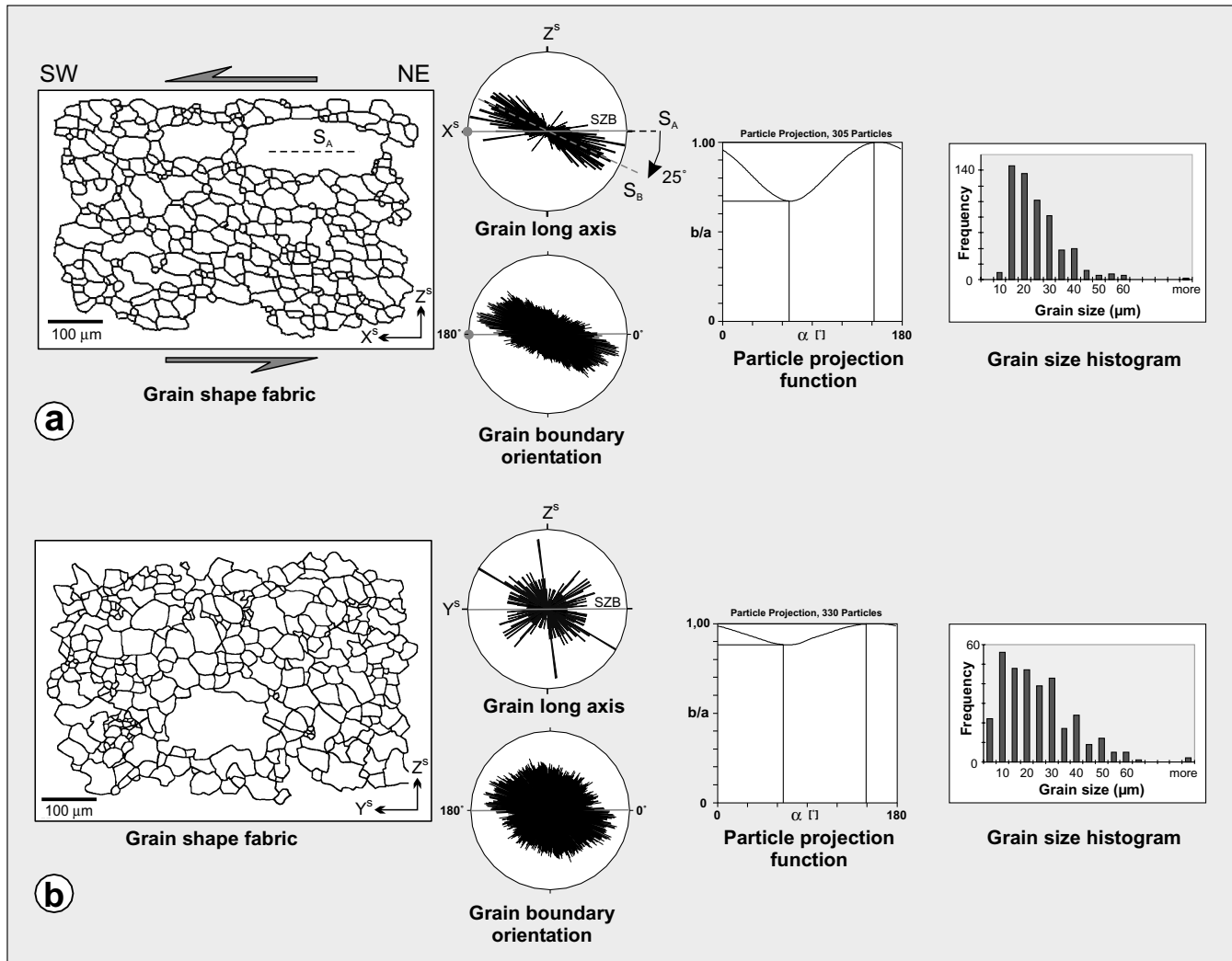
Fig. 8. Digital image analysis (DIAna-software) of the calcite grain shape fabric of the homogeneous dynamically recrystallized ultramylonite sample C 12.1: (a) X^sZ^s-section, S_A = general shear plane, S_B = oblique foliation; (b) Y^sZ^s-section. Grain long axis rose diagrams: Orientation distribution of grain long axes with respect to the SZB. Grain boundary orientation rose diagrams: Orientation of grain boundary segments (200 for each grain) with respect to the SZB. Particle projection function diagrams: Projection lengths of the particles onto the projection line with an angle α (0–180°, anticlockwise counted with respect to the SZB). The average grain ratio b/a and the average angle α of long axis b and short axis a are plotted. This function is a good parameter to quantify grain fabric anisotropy. Grain size histograms: Grain size is given by an equivalent grain diameter of a circle with an area measured for the individual particles. Clear preferred orientation of the grain shape fabric in the X^sZ^s-section. Only a weak grain fabric anisotropy within the Y^sZ^s-section.

preferred grain shape with long axes between 10 and 60 μm in length (mean 25 μm) and average aspect ratio of 1:8. The long axes are preferred oriented at 25° clockwise to the reference plane (Fig. 8a). The shape preferred orientation (SPO) of the homogenous fine-grained matrix thus indicates the characteristic oblique foliation with respect to the reference plane. A nearly isometric grain shape fabric exists in Y^sZ^s-sections, perpendicular to the shear direction (Fig. 8b). Thus, the grain shape and grain boundary fabric reveals a monoclinic symmetry (Fig. 9c) with the two-fold symmetry axis parallel to the Y^s-axis of the sample reference system. The grains are generally not twinned, the extinction is sharp and the boundaries are straight to curved.

The grain shape and boundary geometry of the ultramylonite shows the characteristic oblique foliation fabric (Berthé et al., 1979; Means, 1981; Lister and Snoke, 1984) of monophase mylonites, and indicates the sense of shear in simple shear deformation regimes. The oblique foliation defines the internal fabric S_B (Knipe and Law, 1987) and the main S_A fabric is defined by the mesoscopic white layers. In thin sections, the shear plane is defined by secondary shear bands marked by slight grain size variation, layer parallel luminescence banding, the geometry of asymmetrical quartz grains, and elongated calcite porphyroclasts. The clockwise orientation of the oblique foliation indicates a shear direction of the hanging wall towards SW.

A few remnant calcite porphyroclasts within the fine-grained matrix are observed with long axes oriented parallel to the reference plane. The porphyroclasts have long grain axes in the range of 0.25 to 2 mm with an average aspect
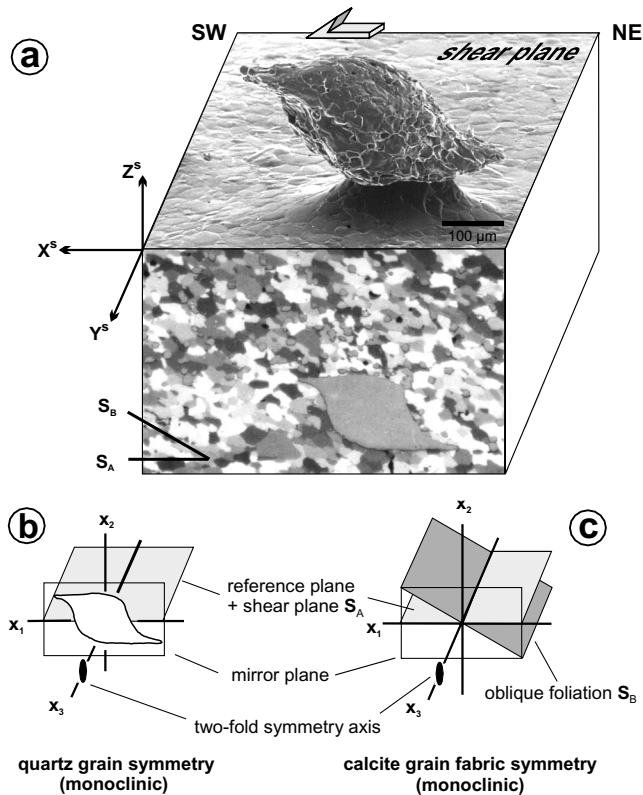
Fig. 9. (a) Geometry of a 'σ-shaped' quartz grain within the calcite ultramylonite matrix and its relation to the sample reference system (S_A, shear plane; S_B, oblique foliation); (b) monoclinic symmetry elements of the quartz grain; (c) monoclinic symmetry elements of the calcite grain fabric (b and c are modified after Passchier and Simpson, 1986).
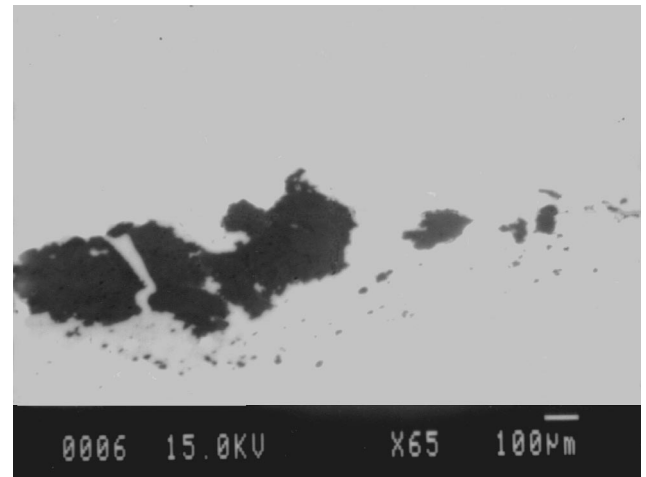

Fig. 10. Backscatter electron image of dolomite aggregates (dark grey) in the calcite matrix (light grey) of the ultramylonite. The large dolomite aggregate is broken into pieces and is oriented with the long axis subparallel to the mylonitic shear plane. Small dolomite grains flow around the larger clasts.

ratio of 1:3. They are often twinned and show undulose extinction.

Secondary shear bands are developed within the homogeneous calcite fabric parallel to the reference plane. These narrow zones of width about 100 μm are defined by a high content of calcite grains smaller than 10 μm.

In cathodoluminescence, red luminescent dolomite first appears in the ultramylonite (< 2 vol.%, see also De Wall et al., 2000, this volume) as rare clasts in the orange–yellow luminescent calcite matrix (Fig. 8-1d in Bestmann, 2000). Their grain sizes range between 10 and 100 μm. Few dolomite aggregates show long axes up to 1 mm. These grains are often fractured (Fig. 10). Some dolomite aggregates are concentrated in horizons parallel to the reference plane and show a characteristic bright luminescence intensity. The typical angular shape indicates brittle behaviour of the dolomite aggregates.

4.3.2. Quartz grains

Quartz grains in the fine-grained calcite matrix show an asymmetric shape (Fig. 5c and d). The grains are flanked by wedge shaped appendages, referred to as 'wings'. The wings extend on both sides of the core parallel to the mylonitic shear plane but do not lie in the same plane. The three-dimensional shape has monoclinic symmetry,

with a two-fold symmetry axis perpendicular to the directions of the wedge shaped wings (Fig. 9a and b) and generally parallel to the Y^s-axis of the external reference system. There are nearly no subgrains in the quartz clasts and wings.

The shape of the quartz grains and their geometric relation to the matrix corresponds to σ_a-type porphyroclasts (Passchier and Simpson, 1986), and are thus called 'σ-shaped' quartz grains. The sense of shear is defined by the tips of the wings pointing to the direction of the relative movement. In other words, the wings step up in the direction of movement of the upper block. The quartz grains extracted by *in situ* etching indicate a shear direction of the hanging wall towards the SW (Fig. 5c and d). The lace network on the quartz surface (Fig. 5d) reflects calcite–calcite–quartz triple junctions and shows the remaining positive relief of the dissolved calcite grains of the ultramylonitic matrix (grain boundary network). The 'σ-shaped' quartz grains are single crystals with a generally uniform extinction (see Bestmann, 2000). The size of the core of the asymmetrical quartz grains varies between 30 and 200 μm. Quartz grains smaller than 30 μm never show this characteristic grain shape. Thus, the development of asymmetric quartz grains seems to be grain size controlled, and grains with similar sizes as those of the fine-grained calcite matrix (10–30 μm) do not show any preferred shape.

4.3.3. Texture

The texture of the fine-grained ultramylonite was measured by fully automatic individual orientation analysis by indexing of EBSD patterns (Adams et al., 1993; Kunze et al., 1994). The experimental set-up at ETH Zürich was as described by Van Daalen et al. (1999). Several 1.5×1.5^2 mm areas from different samples of the homogeneous dynamically recrystallized ultramylonite were scanned on a square grid with a fixed step size of 15 μm. The individual
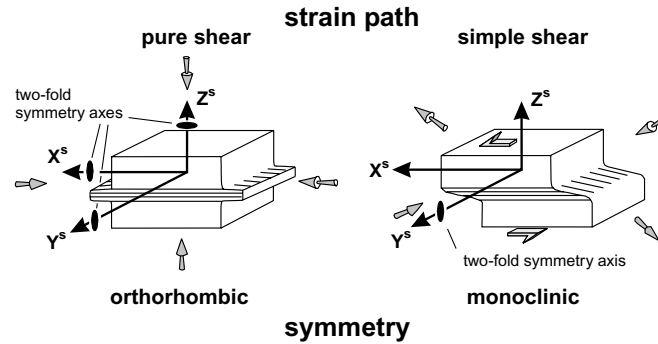
strain path

Fig. 11. Geometry of the two basic strain path models (in plane strain) related to the reference system (X^s-, Y^s-, Z^s-axis) of a shear zone complex. The pure shear system is characterized by three perpendicular two-fold symmetry axes. The simple shear system is characterized by one two-fold symmetry axis parallel to the Y^s-axis.

orientation data were processed by Gaussian convolution with a smoothing width of 15° using the harmonic calculus. From the resulting ODF, pole figures were calculated and presented in a comparable way to those of the coarse-grained samples obtained from neutron diffraction (Fig. 6).

The representative texture of the ultramylonite (C 12.1, Fig. 6c) is characterized by a single c-axis (0001) maximum perpendicular to the reference plane. Compared to the texture in the protolith and protomylonite, no partial girdle of the c-axes is detected in the ultramylonite. The a-axes show a girdle distribution with distinct maxima in the reference plane. Separation of the non-reduced pole figures reveals different positions of the $-a$ [11-20] and $+a$ [-1-120] maxima but none of the a-maxima are parallel to the shear direction. The main difference to the coarse-grained protolith and protomylonite texture is recorded by the $+a$- and $-a$-axis distributions. Whereas both of the separated a-axis pole figures of the protolith and protomylonite show similar girdle distributions, the ultramylonite shows a distribution of distinct maxima, which are at different directions in the two a-axis pole figures. Texture analysis by X-ray diffraction of another ultramylonite sample revealed identical pole figures (Bestmann, 2000) and confirms the data obtained by EBSD.

At first sight, the ultramylonite seems to show a similar texture as the protolith and protomylonite, with the same orthorhombic symmetry. A two-fold symmetry is clearly visible about the Y^s-axis (pole figure center). For orthorhombic symmetry (Fig. 11), a 180° rotation about the Z^s-axis should also result in similar density distributions, which is not the case for the ultramylonite texture.

To test for this symmetry the calcite texture is characterized by two ideal crystal orientations g_A and g_B that represent the main maxima in the orientation distribution (Fig. 12a). They only differ by a 180° rotation around the Z^c-axis. For both orientations, the Z^c-axis of the crystal frame is parallel to the Z^s-axis of the sample frame and thus the c-axes are oriented perpendicular to the reference plane. The specific crystallographic directions of both components are marked in the respective pole figures (Fig. 6c). The two orientations could serve as centers of bell-shaped distribu-

tions with some scattering width and volume fractions, so-called texture components (e.g. Helming et al., 1994; Leiss et al., 1994). The main features of the ultramylonite texture would be well represented by such two components on top of an isotropic background. Obviously, the orientation densities $f(g)$ at both orientations are related by $f(g_A) > f(g_B) > 1$, and similarly would the volume fractions of two respective texture components $v_A > v_B > 0$. While both have a higher density than a random distribution, the A component is stronger than B. Thus the texture of the ultramylonite has clearly no orthorhombic sample symmetry but contains the symmetry elements (a two fold symmetry axis parallel to the Y^s-axis) of a monoclinic sample system (Fig. 11). The ideal orientations are very special as the crystallographic coordinate system coincides with the sample coordinate system ($<c> = Z^c \parallel Z^s$, $<a> = X^c \parallel Y^s$ and $Y^c \parallel X^s$) implying a 'trigonal texture symmetry', because of the trigonal crystal symmetry of calcite. This applies strictly only to the two ideal orientations, but not to the overall ODF. As the two-fold crystal symmetry axis $<a> = X^c$ falls parallel to the reference axis Y^s, it contains a monoclinic texture symmetry. In contrast, there are no two-fold symmetry axes about the Z^s and X^s reference axes, thus no orthorhombic sample symmetry. Evidence for a monoclinic texture is also reflected in pole figures of the rhombs r {10-14} and f {01-12}, which do not show two-fold symmetries about the X^s or Z^s reference axes neither. As both rhomboeder planes contain one of the two-fold a-axes, poles to positive and negative r or f are equivalent by the rotational crystal symmetry and do not need to be separated as for $\pm a$.

Oblique (monoclinic) textures have often been used as reliable shear sense indicators in carbonate rocks (e.g. Wenk et al., 1987; Leiss et al., 1999). For all the calcite textures presented here, the obliquity of the c-axis distributions alone are rather weak to be used as unambiguous shear sense indicators, while the complete orientation distributions are clearly monoclinic or orthorhombic for the ultramylonite or protolith, respectively. Since a CPO must contain all symmetry elements of the deformation causing it, unless it was asymmetric before the deformation event (Paterson and Weiss, 1961), the deformation history of the
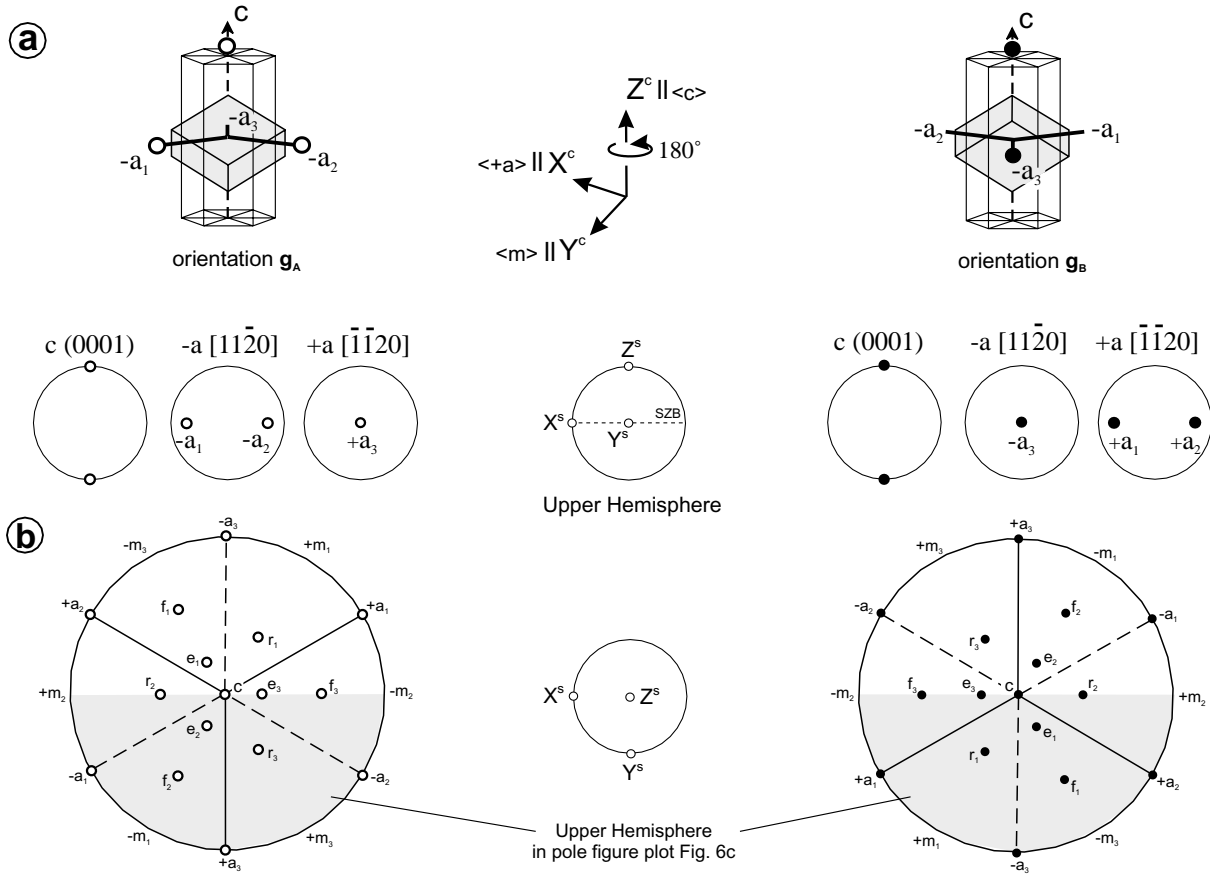
Fig. 12. (a) Ideal crystal orientations g_A (white) and g_B (black) defined by the *c*-axis parallel to the Z^s-axis of the sample frame, and by the different positions of the $-a$ [11-20] axes. The crystal frame (X^c, Y^c, Z^c) is given with respect to the crystal lattice directions ($<+a>$, $<m>$, $<c>$). Stereographic projection (X^cY^c-projection, upper hemisphere) of calcite (modified after Paterson, 1979). The reference frame for pole figures and stereographic projections is given.

ultramylonite can not be higher symmetric than monoclinic, such as simple shear. Finally, the monoclinic CPO of the calcite ultramylonite is consistent with the monoclinic symmetry of the microstructure identified by the calcite grain shape fabric with an oblique foliation and by the 'σ-shaped' quartz grains.

5. Thermometry of dynamic recrystallization

Maximum temperatures between 580 and 620°C were attained in the metamorphic succession during the crustal thickening event. The shear zone development must have occurred at temperatures below this. The almost mono-mineralic marble assemblage provides no clue about the temperature conditions, and instead we infer them from thermometry based on the magnesium content of calcite coexisting with dolomite (Goldsmith and Newton, 1969; Essene, 1983). The method relies on the equilibrium solvus partitioning of magnesium between calcite and dolomite and requires the presence of both phases in the mineral assemblage. Dolomite is absent in the protolith and proto-mylonite and only appears in the highly recrystallized ultra-mylonite as sporadic flakes or enriched in layers up to 100

μm thick that are stretched parallel to the SZB and charac-terized by a bright yellow–orange luminescent colour. The strong localization of the dolomite suggests that its forma-tion was related to exsolution reactions occurring during dynamic recrystallization in the shear zone.

Fig. 13 presents a profile of the relative concentrations X_{MgCO3} in calcite across the protolith, protomylonite and ultramylonite of the shear zone. The X_{MgCO3} value shows a slight, but uniform decrease in the protolith and proto-mylonite, and a slightly more variable decrease in the ultra-mylonite. The total variation is from about $X_{MgCO3} = 0.011$ at the top of the measured profile to about 0.007 at the bottom. The dolomite-enriched area gives $X_{MgCO3} = 0.0095 \pm 0.0017$. Application of the equation of Lieberman and Rice (1986) for the temperature dependence of X_{MgCO3} of the calcite limb of the solvus yields a temperature of $315 \pm 17°C$.

This temperature and the appearance of the dolomite within the ultramylonite can be interpreted in terms of the calcite–dolomite solvus diagram (Fig. 14). During the exhu-mation of the metamorphic complex, the marble underwent retrograde cooling. At temperatures of about 300–350°C calcite marble with X_{MgCO3} of about 0.01 will cross the calcite limb of the solvus into the bi-mineralic field and
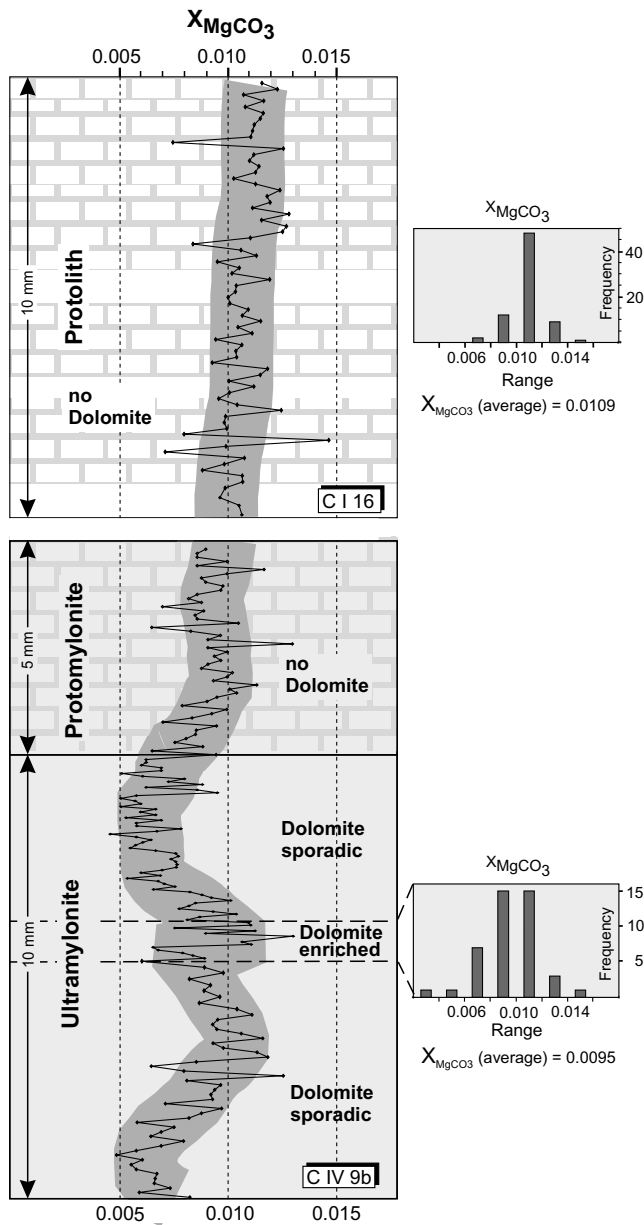
Fig. 13. Combined X_{MgCO_3} profile of the protolith (C I 16) and in the contact zone between protomylonite and ultramylonite (C IV 9b). A trendline with $\Delta X_{MgCO_3} = 0.002$ is shown as dark grey band. The inset X_{MgCO_3} histogram of protolith is based on the values of sample C I 16. The X_{MgCO_3} histogram of the ultramylonite contains compiled data of calcite from 'dolomite enriched area' of sample C IV 9b. The X_{MgCO_3} variation perpendicular to the SZB is probably caused by layer dependent mass transfer of magnesium in flow direction (Bestmann, 2000).

theoretically should undergo exsolution. However, this temperature is below the closure temperature of ca. 500°C for exsolution to occur by cation diffusion (Essene, 1983). Dolomite exsolution only occurs in the ultramylonite, which implies that dynamic recrystallization is the key factor governing the nucleation of dolomite. Less strained rocks such as the protolith and protomylonite do not show any dolomite exsolution. This interpretation indicates that dynamic recrystallization must have been occurring at ca.

300–350°C, i.e. under lower greenschist-facies conditions. Resetting of the dolomite–calcite solvus system induced by dynamic recrystallization was also observed at similar temperatures during alpine thrusting of marbles on the island of Tinos (Matthews et al., 1999).

6. Deformation history

6.1. Evolution of microstructures and textures

The various deformation processes interpreted in the following from microstructures and textures imply significant differences in rheological properties of the differently strained marble rocks (protolith, protomylonite, and ultramylonite). The microstructural observations indicate that the spatial gradient across the shear zone complex may well be interpreted as temporal evolution of the fabric transitions. Although one cannot be certain that the ultramylonite passed through all stages represented by the other fabric domains, some microstructural characteristics of the protolith like relic porphyroclasts are preserved across the microstructural transitions to the ultramylonite (see also Van der Pluijm, 1991; Busch and Van der Pluijm, 1995). The characteristic microstructures of the protolith, protomylonite, and ultramylonite and their kinematic interpretation are schematically compiled in Fig. 15.

6.1.1. Protolith

The coarse-grained protolith seems to have undergone deformation under conditions of relative low strain (based on amount of flattening of the host grains) and high initial stress (based on high twin density) accommodated by twinning (see also Burkhard, 1993). Irregular twin boundaries due to twin boundary migration reflects deformation at temperature well above 300°C (Burkhard, 1993). Additionally, intracrystalline slip (based on undulose extinction and deformation bands) acted as an important deformation mechanism, because twinning can only accommodate a limited amount of strain. The microstructure has orthorhombic symmetry with symmetrically developed sets of twins very similar to those observed in compression experiments of Carrara marble (coaxial deformation) in the twinning regime (e.g. Schmid et al., 1980). The complete CPO with a single *c*-axis maximum perpendicular to the reference plane and *a*-axis girdle within this plane reveals a nearly orthorhombic symmetry as well. The weak *c*-axis girdles normal to the sample X^s-direction (along with *a*-axis maxima parallel to X^s) are evidence of a true triaxial (still non-rotational) strain path as opposed to a uniaxial compressional regime, since the latter should have resulted in an axialsymmetric fabric. The obliquities of these *c*-axis girdles (with different orientation with respect to the $Y^s Z^s$-plane, Fig. 6a) can not be related to a specific sense of shear, as it was described for sheared dolomite marble by Leiss et al. (1994). Microstructure and the CPO of the marble
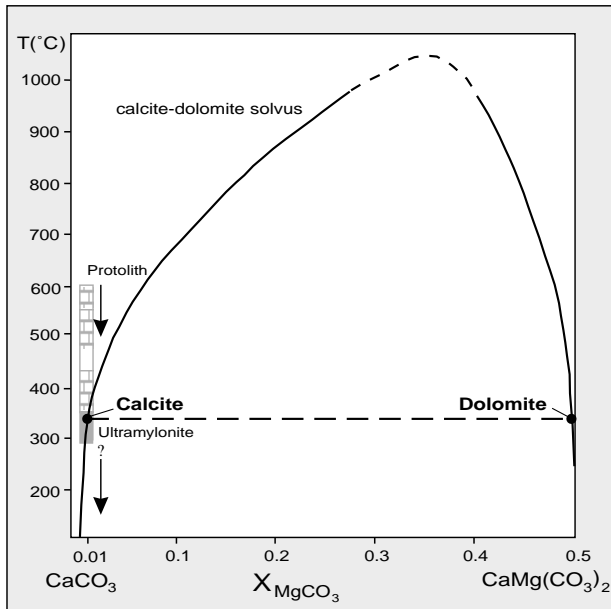
Fig. 14. Cooling history model of the shear zone complex, based on the calcite-dolomite solvus (after Anovitz and Essene, 1987). Temperature estimation is based on the dolomite exsolution reaction from Mg-calcite ($X_{MgCO_3} \sim 0.01$) during pervasive dynamic recrystallization.

protolith are comparable with the patterns of experimentally deformed calcite marble under low temperature, coaxial conditions in the twinning regime (Schmid et al., 1980; Wenk, 1985; Wenk et al., 1987). There is a good agreement with simulated textures (Wenk et al., 1987) based on e-twinning and *r*-slip as the dominant deformation mechanisms. It is thus concluded that the coarse-grained marble outside the mylonitic shear zone recorded a dominant co-axial deformation which probably led to subvertical thinning of the entire calcite marble complex (see also Fassoulas et al., 1994).

6.1.2. Protomylonite

'Core and mantle' structures are the characteristic features of the protomylonite indicating further deformation along with subgrain rotation recrystallization (White, 1976). Strong undulose extinction and high density of low-angle boundaries suggest intense intracrystalline deformation within the coarse grains of the protomylonite. A gradual transition of aggregates of subgrains ($\omega_{nm} < 15°$) at the margin of clasts to aggregates of new grains ($\omega_{nm} > 15°$, free of twins and with sharp extinction) with approximately the same grain size (Fig. 7) indicates subgrain rotation as the recrystallization mechanism resulting in a major grain size reduction. The SPO of the grains and a single dominant twin set in the porphyroclasts are oblique to the SZB, revealing a monoclinic fabric symmetry, which gives evidence of a non-coaxial strain component in the protomylonite. Similar oblique 'core and mantle' structures were observed by Pieri (1999) and Pieri et al. (2000) in Carrara marble

deformed to shear strains $\gamma = 2$ to 5 in high temperature torsion experiments.

The texture of the protomylonite is nearly identical to that of the protolith. For non-coaxial deformation it is expected that twinning would reorient the calcite *c*-axes against the sense of shear (Schmid et al., 1987). The texture of the protomylonite shows only a slight asymmetry even with the sense of shear related to the SZB, but too little to be considered representative. It still preserves the internal orthorhombic texture symmetry of the protolith, just rigidly rotated slightly. The observed dominance of one twin set is interpreted as left over remnant of the former protolith microstructure, where the less favourably oriented twins with respect to the non-coaxial deformation regime were wiped out by twin boundary migration recrystallization in the protomylonite. Rutter et al. (1994) showed that an initial twinning texture of experimental deformed calcite marbles can survive during annealing and a second deformation phase. Similarly, the orthorhombic fabric of the coarse protolith grains still dominates the protomylonite CPO, with no major modification by the dynamically recrystal-lized grains so far. The non-coaxial strain component clearly visible in the microstructure, is not yet documented in the CPO.

6.1.3. Ultramylonite

The fine-grained ultramylonite in the interior of the shear zone had completely recrystallized. The homogeneous microstructure may represent microstructural 'steady state' flow conditions (e.g. Ree, 1991; Herwegh and Handy, 1998). The interior of the recrystallized grains is generally free of twins. Therefore, twinning does not contribute to the deformation of the fine-grained ultramylonite, in contrast to the protolith and the protomylonite. The SPO with an oblique foliation indicates dominant non-coaxial homogeneous plastic flow within the shear zone, possibly accompanied by some thinning perpendicular to the SZB (see also Herwegh and Handy, 1998). The asymmetric ('σ-shaped') quartz grains with wedge shaped appendages correspond to a top-to-SW shear direction in the fine-grained ultramylonite. Thus the three-dimensional shape of the quartz grains, the three-dimensional analysis of the calcite grain shape fabric in X^sZ^s- and Y^sZ^s-section and the calcite CPO reveal a monoclinic fabric symmetry. They provide evidence for dominant non-coaxial deformation under approximately plane strain conditions during strain localization in the shear zone.

Compared with experimental deformation textures, the texture of the Thassos ultramylonite is similar but not equal to that of limestones deformed at low-temperature (LT) pure shear conditions (reviewed by Wenk et al., 1987), and at high temperature (HT) simple shear (Schmid et al., 1987). All textures compare well in a strong *c*-axis maximum perpendicular to the SZB and an *a*-axis girdle within the reference plane. They differ in that the *a*-axes were more evenly distributed along this girdle than in the
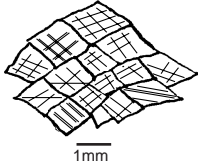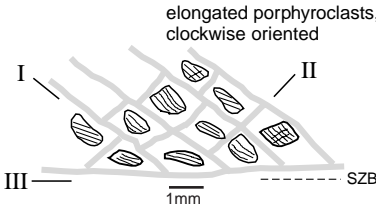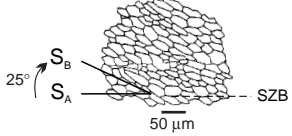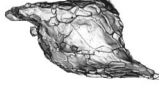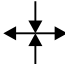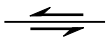
	PROTOLITH	**PROTOMYLONITE**	**ULTRAMYLONITE**
twinning	1, 2 or 3 twin sets two dominant twin orientations (clockwise and anticlockwise)	2 twin sets (only in porphyroclasts) one dominant twin orientation (clockwise)	no twins
shape preferred orientation	 1mm	elongated porphyroclasts, clockwise oriented 1mm	'steady state' fabric with oblique foliation of the dynamically recrystallized grain fabric (20-30° clockwise oriented to the SZB) 50 µm
dynamic recrystal-lization	rare, along grain boundaries	'core and mantle structure' + 3 sets (I-III) of recrystallization bands (grey lines; set 'I' is dominant)	pervasive dynamic recrystallization
quartz grains			
microfabric symmetry	microstructure: orthorhombic texture: orthorhombic	microstructure: monoclinic texture: " orthorhombic	microstructure: monoclinic texture: monoclinic
deformation mechanisms	twinning + intracrystalline slip	twinning + intracrystalline slip + subgrain rotation recrystallization	duplex basal <a> slip accompanied by pervasive dynamic recrystallization
strain path	pure shear	first evidence of a component of simple shear	simple shear

Fig. 15. Schematic compilation of microstructures and their kinematic significance for the Thassos marble shear zone complex. Microfabric symmetry and corresponding dominant strain path (pure shear vs. simple shear) are given. Interpretation of dominant deformation mechanisms is based on the comparison with experimental microfabrics and simulated textures. Microstructures are presented in $X^s Z^s$-sections (SZB shear zone boundary). Within the coarse grained protolith and protomylonite both spherical and ellipsoidal/oblong shapes of quartz grains are common.

ultramylonite. However, microstructures indicative of pervasive dynamic recrystallization only occur within the grain boundary migration regime in the HT experiments under simple shear conditions (Friedman and Higgs, 1981; Schmid et al., 1987), which are believed to simulate microstructural and textural fabrics of greenschist facies calcite mylonite zones under geologically realistic strain rates (LaFrance et al., 1994).

It has been suggested that slip systems tend to rotate into an orientation that maximizes the resolved shear stress in the slip direction (Schmid and Casey, 1986). At 'steady state' (time independent) flow, this concept predicts a stable end orientation of the 'easiest' slip systems parallel to the bulk shear direction, within glide planes oriented parallel to the shear zone boundary (e.g. Etchecopar and Vasseur, 1987). This process is promoted by pervasive dynamic recrystallization (Schmid and Casey, 1986; Schmid, 1994). Schmid et al. (1987) considered basal slip in the *a*-direction to be the

dominant slip system in the grain boundary migration regime, according to one of the *a*-axis maxima of the experimental texture oriented parallel to the shear direction. In case of the Thassos ultramylonite, none of the three *a*-axis maxima is aligned with the shear direction, but a pole to the *m*-plane (Fig. 12b). If the preferred orientation would result from a single active slip system as the 'orientation of easy slip', then a slip system $(0001) < 10\text{-}10 > \ (= \text{basal-}m)$ would have produced this texture. But basal-*m* slip has never been reported for calcite. The 'easy slip' model could be modified by simultaneous activation of more than one of the existing basal-*a* slip systems (De Bresser, 1991). If for example $-a_1$ and $+a_2$ are active, these *a*-axis directions will be oriented at 30° relative to the shear direction, as often observed also for quartz textures (Schmid and Casey, 1986).

As noted above the ideal crystal orientation g_B is less present than the orientation g_A in the orientation distribution.

Though any crystallographic direction is inversion symmetric due to the inversion center of the calcite structure, the two orientations g_A and g_B are obviously not equivalent with respect to the sense of shear, as shown by the different positions of rhombs r {10-14} and f {01-12} or e {01-18} twin planes (Fig. 12b). For glide on the basal-a slip system both orientations are energetically equivalent, but even minor contributions of slip on rhomb systems can make g_A more favourable than g_B. The wide scatter of the orientation components is attributed to lattice bending due to intracrystalline deformation and texture randomization through recrystallization and diffusional processes.

In summary, the ultramylonite possesses a 'steady state' microstructure and CPO. The single c-axis maximum perpendicular to the shear foliation and the specific a-axis maxima at a 30° angle relative to the shear direction can be result of duplex slip on different a-directions on the basal plane in a non-coaxial deformation regime.

6.2. Kinematic model

The Thassos shear zone complex reveals a strain/strain path gradient that is accompanied by a change in the deformation processes across the shear zone profile. In other words, the different rock types (protolith, protomylonite, and ultramylonite) have seen different strains under different strain regimes, and must have shown different rheological behaviour during deformation. It seems probable that the entire calcite marble complex has undergone a component of early coaxial deformation during the uplift of the metamorphic core complex (Fig. 16 (1)) which led to subvertical thinning in an already extensional deformation regime (see also Lister and Davis, 1989; Fassoulas et al.,
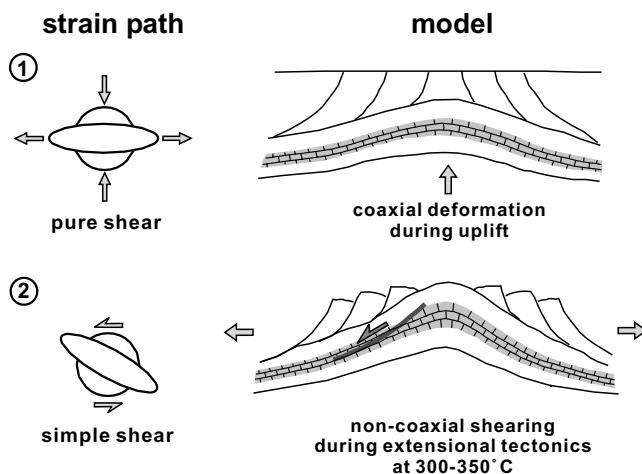

Fig. 16. Simplified sketch illustrating the evolution of the calcite marble shear zone complex in the context to the Thassos metamorphic core complex. (1) The entire calcite marble complex underwent a component of early coaxial deformation during the uplift of the metamorphic core complex. (2) During extensional tectonics, strain localization occurred in response to decreasing $P–T$ conditions. The shallow dipping shear zone cuts through the 'already' deformed coarse-grained calcite marble complex. High strain is accommodated together with non-coaxial flow.

1994). During foreland-directed extensional tectonics under retrograde conditions (300–350°C), strain concentration resulted in the localization of deformation in narrow zones. Therefore, the shallow-dipping shear zone cuts through the 'already' deformed coarse-grained calcite marble (Fig. 16 (2)). This simple shear event is not recorded in the protolith marble. As Hobbs et al. (1990) pointed out, relatively undeformed rocks surrounding shear zones show a more elastic and limited plastic rheological behaviour, compared to plastically deformed shear zone rocks. Some non-coaxial deformation components on the protolith can not be completely ruled out, but their effects are not obvious. The first evidence of a component of heterogeneous simple shear deformation is recorded within the protomylonite. Enhanced strain weakening promotes high localization of plastic deformation in the shear zone, where the high strains are accommodated by dynamic recrystallization and non-coaxial flow (Rutter, 1999). The ultramylonite takes up most of the shear strain, and the protomylonite rocks within the shear zone surrounded by the ultramylonites are probably deformed more slowly and record less non-coaxiality.

Thus the different strain paths observed in the protolith and ultramylonite are related to subsequent deformation events as opposed to 'true' strain path partitioning (e.g. Sanderson, 1976; Means, 1994) where the imposed bulk strain path is simultaneously distributed in a coaxial component mainly accommodated outside the shear zone and a non-coaxial component within the shear zone.

6.3. Strain localization

Localization of deformation can occur if, e.g., the rock strength in the shear zone is less than that of the host rock (Rutter, 1999). In lithologically heterogeneous rocks, strain gradients may arise at the interface between contrasting materials and may laterally propagate into homogeneous material (Rutter, 1999) and/or the deformation will be preferentially localized in incompetent layers (e.g. schist, Lister and Williams, 1983). The calcite shear zone of this study is developed within a rather 'homogeneous' calcite marble complex, with no visible compositional or structural variations at outcrop scale. Wang et al. (1996) infer from experiments on calcite single crystals, that deformation may be localized in a particular marble layer of slightly different chemical composition (e.g. with different Mn content). Cathodoluminescence of the protolith reveal some layer parallel compositional differences parallel to the SZB although the layer-specific chemical differences were too minor to be identified (Bestmann, 2000). Together with local microstructural variations, such zones of presumed slightly different composition may have initiated the strain-weakening. This resulted in the development of 'layer-parallel' shear zones (referred to as main foliation of the protolith, SZB plane, and mylonitic shear plane). Further deformation became easier in these already

deformed zones, rather than initiate deformation elsewhere (Poirier, 1980). The sharp shear zone boundary of the complex implies rapid strain weakening (Brodie and Rutter, 1987).

7. Conclusions

The strain regime (amount of coaxial flow relative to non-coaxial flow) of naturally deformed calcite marbles is often estimated from the degree of asymmetry of the texture, defined by the angular displacement of the *c*-axis maximum from the normal of the SZB (Wenk et al., 1987; Ratschbacher et al., 1991; Erskine et al., 1993; Leiss et al., 1999). This study of the Thassos marble shear zone complex demonstrates that pure shear, as well as simple shear strain paths, can produce similar looking c-axis fabrics by different dominant deformation processes. A single *c*-axis maximum perpendicular to the SZB is shown for both the coarse-grained protolith (twinning + intracrystalline slip) deformed in pure shear and the fine-grained ultramylonite (dynamic recrystallization + intracrystalline slip) deformed in simple shear. The textures of carbonate rocks are frequently interpreted by their *c*-axes distributions, and both *a*-axes −*a* [11-20] and +*a* [-1-120] are often summarized in one (inversion symmetric) pole figure of ±a <11-20 >. For the ultramylonite texture, such a presentation would suggest an apparently orthorhombic distribution, and could have led to wrong interpretations such as coaxial deformation for the ultramylonite, or an inherited texture from the deformed protolith marble. From the crystallographic point of view, −*a*-axes and +*a*-axes define different crystal orientation of calcite grains within a polycrystal aggregate (Fig. 12). In this study, separated *a*-axis pole figures show different density distributions, indicating orthorhombic texture symmetry for the protolith and monoclinic symmetry for the ultramylonite. It was observed that during dominant non-coaxial deformation occurring together with pervasive dynamic recrystallization, the resultant *c*-axis maximum, was not deflected with respect to the SZB, but that different *a*-axes distributions broke the orthorhombic texture symmetry. Furthermore, even where the microstructures indicated a change in the deformation kinematics (from coaxial to non-coaxial deformation) as from the protolith to the protomylonite, the texture did not change immediately. Therefore, texture as a possible shear sense or strain path indicator in naturally deformed calcite marbles is not necessarily unambiguous, but more sensitive if the complete crystallographic orientation is considered. Microstructures are much more sensitive and reliable features, responding more immediate to continuous changes in deformation conditions.

It is concluded that non-coaxial deformation becomes more important with increasing strain and results in a 'steady state' flow fabric in the pervasively recrystallized ultramylonite. Dynamic recrystallization plays the most important role in the evolution of the Thassos calcite shear zone complex. Dynamic recrystallization and the accompanying intracrystalline deformation mechanisms led to (1) grain size reduction, (2) strain weakening and strain localization, (3) exsolution reaction of dolomite from calcite and (4) the development of a 'steady state' microfabric with flow planes parallel to the shear zone boundary.

References

Adams, B.L., Wright, S.I., Kunze, K., 1993. Orientation imaging: The emergence of a new microscopy. Metallurgical Transactions 24A, 819–831.

Anovitz, L.M., Essene, E.J., 1987. Phase Equilibria in the System CaCO₃–MgCO₃–FeCO₃. Journal of Petrology 28, 389–414.

Bestmann, M., 2000. Evolution of a shear zone in calcite marble on Thassos Island, Northern Greece: results from microfabrics and stable isotopes. Erlanger geologische Abhandlungen 131, 1–127.

Berthé, D., Choukroune, P., Jegouzo, P., 1979. Orthogneiss, mylonite and non coaxial deformation of granites: the example of the South American Shear-Zone. Journal of Structural Geology 1, 31–42.

Brodie, K.H., Rutter, E.H., 1987. Deep crustal extensional faulting in the Ivrea zone of northern Italy. Tectonophysics 140, 193–212.

Burkhard, M., 1990. Ductile deformation mechanisms in micritic limestones naturally deformed at low temperatures (150–350°C). In: Knipe, R.J., Rutter, E.H. (Eds.), Deformation Mechanisms, Rheology and Tectonics. Geological Society Special Publication 54, pp. 241–257.

Burkhard, M., 1993. Calcite twins, their geometry, appearance and significance as stress-strain markers and indicators of tectonic regime: a review. Journal of Structural Geology 15, 351–368.

Busch, J.P., Van der Pluijm, B.A., 1995. Calcite textures, microstructures and rheological properties of marble mylonites in the Bancroft shear zone, Ontario, Canada. Journal of Structural Geology 17, 677–688.

Covey-Crump, S.J., Rutter, E.H., 1989. Thermally-induced grain growth of

calcite marbles on Naxos Island. Contributions to Mineralogy and Petrology 120, 282–310.

De Bresser, J.H.P., 1991. Intracrystalline deformation of calcite. Geologica Ultraiectina 79, 1–191.

De Wall, H., Bestmann, M., Ullemeyer, K., 2000. Anisotropy of diamagnetic susceptibility in Thassos marble: A comparison between measured and modelled data. Journal of Structural Geology 22, 1761–1771.

Dinter, D.A., 1998. Late Cenozoic extension of the Alpine collisional orogen, northeastern Greece: Origin of the north Aegean basin. Geological Society of America Bulletin 110, 1208–1230.

Dinter, D.A., Royden, L., 1993. Late Cenozoic extension in the northeastern Greece: Strymon Valley detachment and Rhodope metamorphic core complex. Geology 21, 45–48.

Erskine, B.G., Heidelbach, F., Wenk, H.-R., 1993. Lattice preferred orientations and microstructures of deformed Cordilleran marbles: correlation of pure shear indicators and determination of strain path. Journal of Structural Geology 15, 1189–1205.

Essene, E.J., 1983. Solid solution and solvi among metamorphic carbonates with application to geologic thermometry. In: Reeder, R.J. (Ed.), Reviews in Mineralogy and Chemistry: Carbonates. Mineralogical Society of America 11, pp. 77–96.

Etchecopar, A., Vasseur, G., 1987. A 3-D kinematic model of fabric development in polycrystalline aggregates: comparison with experimental and natural examples. Journal of Structural Geology 9, 705–717.

Fassoulas, C., Kilias, A., Mountrakis, D., 1994. Postnappe stacking extension and exhumation of high-pressure/low-temperature rocks in the island of Crete, Greece. Tectonics 13, 127–138.

Friedman, M., Higgs, N.G., 1981. Calcite fabrics in experimental shear zones. In: Carter, N.L., Friedman, M., Logan, J.M., Stearns, D.W. (Eds.), Mechanical Behaviour of Crustal Rocks—the Handin Volume. American Geophysical Union, Geophysical Monograph 24, pp. 11–27.

Goldsmith, J.R., Newton, R.C., 1969. P–T–X relations in the system $CaCO_3$–$MgCO_3$ and high temperatures and pressures. American Journal of Science 267A, 160–190.

Helming, K., Wenk, H.-R., Choi, C.S., Schäfer, W., 1994. Description of quartz textures by components. Examples from metamorphic rocks. In: Bunge, H.J., Siegesmund, S., Skrotzki, W., Weber, K. (Eds.), Textures of Geological Materials, DGM Informationsgesellschaft, Oberusel, pp. 303–326.

Herwegh, M., Handy, M.R., 1998. The origin of shape preferred orientations in mylonite: inference from in-situ experiments on polycrystalline norcamphor. Journal of Structural Geology 20, 681–694.

Hobbs, B.E., Mühlhaus, H.-B., Ord, A., 1990. Instability, softening and localization of deformation. In: Knipe, R.J., Rutter, E.H. (Eds.), Deformation Mechanisms, Rheology and Tectonics. Geological Society Special Publication 54, pp. 143–165.

Kilias, A., Falalakis, G., Mountrakis, D., 1999. Cretaceous-Tertiary structures and kinematics of the Serbomacedonian metamorphic rocks and their relation to the exhumation of the Hellenic hinterland (Macedonia, Greece). International Journal of Earth Sciences 88, 513–531.

Knipe, R.J., Law, R.D., 1987. The influence of crystallographic orientation and grain boundary migration on microstructural and textural evolution in an S–C mylonite. Tectonophysics 135, 155–169.

Kunze, K., Heidelbach, F., Wenk, H.-R., Adams, B.L., 1994. Orientation Imaging Microscopy of Calcite Rocks. In: Bunge, H.J., Siegesmund, S., Skrotzki, W., Weber, K. (Eds.), Textures of Geological Materials, DGM Informationsgesellschaft, Oberusel, pp. 279–302.

LaFrance, B., White, J.C., Williams, P.F., 1994. Natural calcite c-axis fabrics; an alternative explanation. Tectonophysics 229, 1–18.

Leiss, B., Siegesmund, S., Weber, K., Olesen, N.O., 1994. Localized texture components of a naturally deformed dolomite—a contribution to the analysis of texture-forming processes. In: Bunge, H.J., Siegesmund, S., Skrotzki, W., Weber, K. (Eds.), Textures of Geological Materials, DGM Informationsgesellschaft, Oberusel, pp. 261–275.

Leiss, B., Siegesmund, S., Weber, K., 1999. Texture asymmetries as shear sense indicators in naturally deformed mono- and polyphase carbonate rocks. Textures and Microstructures 33, 61–74.

Lieberman, J.E., Rice, J.M., 1986. Petrology of marble and peridotite in the Seiad ultramafic complex, northern California, USA. Journal of Metamorphic Geology 4, 179–199.

Lister, G.S., Davis, G.A., 1989. The origin of metamorphic core complexes and detachment faults formed during Tertiary continental extension in the northern Colorado River region, U.S.A. Journal of Structural Geology 11, 65–94.

Lister, G.S., Snoke, A.W., 1984. S–C mylonites. Journal of Structural Geology 6, 617–638.

Lister, G.S., Williams, P.F., 1983. The partitioning of the deformation in flowing rock masses. Tectonophysics 92, 1–33.

Matthews, A., Lieberman, J., Avigad, D., Garfunkel, Z., 1999. Fluid-rock interaction and thermal evolution during thrusting of an Alpine metamorphic Complex. Contributions to Mineralogy and Petrology 135, 212–224.

Matthies, S., Vinel, G.W., 1982. On the reproduction of the orientation distribution function of textured samples from reduced pole figures using the conception of a conditional ghost correction. Physical Status Solidi (b) 112, K111–K120.

Means, W.D., 1981. The concept of steady-state foliation. Tectonophysics 78, 179–199.

Means, W.D., 1994. Rotational quantities in homogeneous flow and the development of small-scale structures. Journal of Structural Geology 16, 437–445.

Papanikolaou, D., 1984. The three metamorphic belts of the Hellenides: a review and a kinematic interpretation. In: Dixon, J.E., Robertson, A.H.F. (Eds.), Geological Evolution of the Eastern Mediterranean. Geological Society of London Special Publication 17, pp. 551–561.

Passchier, C.W., Simpson, C., 1986. Porphyroclast systems as kinematic indicators. Journal of Structural Geology 8, 895–910.

Paterson, M.S., 1979. Deformation Mechanisms in Carbonate Crystals. In: Borland, D.W., Clarebrough, L.M., Moore, A.J.W. (Eds.), Physics of Materials (A festschrift for Dr. Walter Boas), CSIRO and University of Melbourne, Melbourne, pp. 199–208.

Paterson, M.S., Weiss, L.E., 1961. Symmetry concepts in the structural analysis of deformed rocks. Geological Society America Bulletin 72, 841–882.

Peterek, A., Polte, M., Wölfl, C., Bestmann, M., Lemtis, O., 1994. Zur jungtertiären geologischen Entwicklung im SW der Insel Thassos (S-Rhodope, Nordgriechenland). Erlanger Geologische Abhandlungen 124, 29–59.

Pieri, M., 1999. Shear deformation of calcite rocks. Rheology and microfabric evolution of Carrara marble under dynamic recrystallization during torsion experiments. Ph.D. thesis ETH Zurich.

Pieri, M., Stretton, I., Kunze, K., Burlini, L., Olgaard, D.L., Burg, J.-P., Wenk, H.-R., 2000. Texture development in calcite through deformation and dynamic recrystallization during torsion to large strains. Tectonophysics (in press).

Poirier, J.P., 1980. Shear localization and shear instability in materials in the ductile field. Journal of Structural Geology 2, 135–142.

Ramsay, J.G., 1980. Shear zone geometry: a review. Journal of Structural Geology 2, 83–99.

Ratschbacher, L., Wenk, H.-R., Sintubin, M., 1991. Calcite textures: examples from nappes with strain-path partitioning. Journal of Structural Geology 13, 369–384.

Ree, J.-H., 1991. An experimental steady-state foliation. Journal of Structural Geology 13, 1001–1011.

Rutter, E.H., 1999. On the relationship between the formation of shear zones and the form of the flow law for rocks undergoing dynamic recrystallization. Tectonophysics 303, 147–158.

Rutter, E.H., Casey, M., Burlini, L., 1994. Preferred crystallographic orientation development during the plastic and superplastic flow of calcite rocks. Journal of Structural Geology 10, 1431–1446.

Sanderson, D.J., 1976. The superposition of compaction and plane strain. Tectonophysics 30, 35–54.

Schmid, S.M., 1994. Textures of geological materials: computer model predictions versus empirical interpretations based on rock deformation experiments and field studies. In: Bunge, H.J., Siegesmund, S., Skrotzki, W., Weber, K. (Eds.), Textures of Geological Materials, DGM Informationsgesellschaft, Oberusel, pp. 279–302.

Schmid, S.M., Casey, M., 1986. Complete fabric analysis of some commonly observed quartz C-axis patterns. Geophysical Monographs 36, 263–286.

Schmid, S.M., Panozzo, R., Bauer, S., 1987. Simple shear experiments on calcite rocks: rheology and microfabric. Journal of Structural Geology 9, 747–778.

Schmid, S.M., Paterson, M.S., Boland, J.N., 1980. High temperature flow and dynamic recrystallization in Carrara marble. Tectonophysics 65, 245–280.

Schulz, B., 1992. Syntectonic heating and loading-deduced from microstructures and mineral chemistry in micaschists and amphibolites of the Pangeon complex (Thassos island, Northern Greece). Neues Jahrbuch für Geologie und Paläontologie Abhandlungen 184, 181–201.

Sibson, R.H., 1977. Fault rocks and fault mechanisms. Journal of the Geological Society of London 133, 191–213.

Tullis, J., 1983. Deformation of feldspars. In: Ribbe, P.H. (Ed.), Feldspar Mineralogy. Reviews in Mineralogy, Volume 2. Mineralogical Society of America, pp. 297–323.

Ullemeyer, K., Spalthoff, P., Heinitz, J., Isakov, N.N., Weber, K., 1998. The SKAT texture diffractometer at the pulsed reactor IBR-2 at Dubna: experimental layout and first measurements. Nuclear Instrumental Methods of Physical Research A 412/1, 80–88.

Van Daalen, M., Heilbronner, R., Kunze, K., 1999. Orientation analysis of localized shear deformation in quartz fibres at the brittle-ductile transition. Tectonophysics 303, 83–107.

Van der Pluijm, B.A., 1991. Marble mylonites in the Bancroft shear zone, Ontario, Canada: microstructures and deformation mechanisms. Journal of Structural Geology 13, 1125–1135.

Voll, G., 1976. Recrystallization of quartz, biotite, feldspars from Erstfeld to the Leventina Nappe, Swiss Alps, and its geological significance. Schweizer mineralogische und petrographische Mitteilungen 56, 641–647.

Wang, Z.-C., Bai, Q., Dresen, G., Wirth, R., 1996. High-temperature deformation of calcite single crystals. Journal of Geophysical Research, 101, 20,377–20,390.

Wawrzenitz, N., Krohe, A., 1998. Exhumation and doming of the Thassos metamorphic core complex (S Rhodope, Greece): structural and geochronological constraints. Tectonophysics 285, 301–332.

Wenk, H.-R., 1985. Preferred Orientation in Deformed Metals and Rocks: An Introduction to Modern Texture Analysis. Academic Press, Orlando.

Wenk, H.-R., Christie, J.M., 1991. Comments on the interpretation of deformation textures in rocks. Journal of Structural Geology 13, 1091–1110.

Wenk, H.R., Matthies, S., Donovan, J., Chateigner, D., 1998. BEARTEX: A windows-based program system for quantitative texture analysis. Journal of Applied Crystallography 31, 262–269.

Wenk, H.-R., Takeshita, T., Bechler, E., Erskine, B.G., Matthies, S., 1987. Pure shear and simple shear calcite textures. Comparison of experimental, theoretical and natural data. Journal of Structural Geology 9, 731–745.

White, S.H., 1976. The effect of strain on the microstructures, fabrics, and deformation mechanisms in quartzites. Philosophical Transactions of the Royal Society of London A283, 69–86.